A&A 663, A167 (2022)
https://doi.org/10.1051/0004-6361/202243943

Astronomy & Astrophysics

New DA white dwarf models for asteroseismology of ZZ Ceti stars

Leandro G. Althaus[1,2] and Alejandro H. Córsico[1,2]

[1] Grupo de Evolución Estelar y Pulsaciones, Facultad de Ciencias Astronómicas y Geofísicas, Universidad Nacional de La Plata, Paseo del Bosque s/n, 1900 La Plata, Argentina
e-mail: althaus@fcaglp.unlp.edu.ar
[2] IALP – CONICET, La Plata, Argentina

Received 3 May 2022 / Accepted 27 May 2022

ABSTRACT

Context. Asteroseismology is a powerful tool used to infer the evolutionary status and chemical stratification of white dwarf stars and to gain insights into the physical processes that lead to their formation. This is particularly true for the variable hydrogen-rich atmosphere (DA) white dwarfs, known as DAV or ZZ Ceti stars. They constitute the most numerous class of pulsating white dwarfs.
Aims. We present a new grid of white dwarf models that take into account advances made over the last decade in modeling and input physics of both the progenitor and the white dwarf stars. As a result, it is possible to avoid several shortcomings present in the set of white dwarf models employed in the asteroseismological analyses of ZZ Ceti stars that we carried out in our previous works.
Methods. We generate white dwarf stellar models appropriate for ZZ Ceti stars with masses from ∼0.52 to ∼0.83 $M_{\odot}$, resulting from the whole evolution of initially 1.5–4.0 $M_{\odot}$ mass star models. These new models are derived from a self-consistent way with the changes in the internal chemical distribution that result from the mixing of all the core chemical components induced by mean molecular-weight inversions, from ^{22}Ne diffusion, Coulomb sedimentation, and from residual nuclear burning. In addition, the expected nuclear-burning history and mixing events along the progenitor evolution are accounted for, in particular the occurrence of third dredge-up, which determines the properties of the core and envelope of post-AGB and white dwarf stars, as well as the white dwarf initial-final mass relation. The range of hydrogen envelopes of our new ZZ Ceti models extends from the maximum residual hydrogen content predicted by the progenitor history, $\log(M_{\rm H}/M_{\odot}) \sim -4$ to -5, to $\log(M_{\rm H}/M_{\odot}) = -13.5$, thus allowing for the first stellar models that would enable the search for seismological solutions for ZZ Ceti stars with extremely thin hydrogen envelopes – if, indeed, they do exist in nature. We computed the adiabatic gravity(g)-mode pulsation periods of these models. Calculations of our new evolutionary and pulsational ZZ Ceti models were performed with the LPCODE stellar evolution code and the LP-PUL stellar pulsation code.
Results. Our new hydrogen-burning post-AGB models predict chemical structures for ZZ Ceti stars that are substantially different from those we used in our previous works, particularly in connection with the chemical profiles of oxygen and carbon near the stellar centre. We also discuss the implications of these new models for the pulsational spectrum of ZZ Ceti stars. Specifically, we find that the pulsation periods of g modes and the mode-trapping properties of the new models differ significantly from those characterizing the ZZ Ceti models of our previous works, particularly for long periods.
Conclusions. The improvements in the modeling of ZZ Ceti stars we present here lead to substantial differences in the predicted pulsational properties of ZZ Ceti stars, which are expected to impact the asteroseismological inferences of these stars. This is extremely relevant in view of the abundant amount of photometric data from current and future space missions, resulting in discoveries of numerous ZZ Ceti stars.

Key words. stars: evolution – stars: interiors – white dwarfs – stars: oscillations – asteroseismology

1. Introduction

Most stars exhibit pulsational instabilities at some stage of their evolution. Asteroseismology constitutes a powerful and unique tool that allows us to extract key information about their internal structure by comparing the independent periods present in their pulsation spectrum with those predicted by theoretical pulsation models (Unno et al. 1989; Catelan & Smith 2015; Aerts 2021; Kurtz 2022). In the field of white dwarf (WD) stars, this technique has proved to be extremely useful for inferring the evolutionary status and the internal chemical stratification of these stars (Córsico et al. 2019). In particular, WDs with hydrogen(H)-rich atmospheres (DA spectroscopic class) exhibit pulsational instabilities in a narrow strip, with effective temperatures of 10 400 K $\lesssim T_{\rm eff} \lesssim$ 12 400 K and surface gravities $7.5 \lesssim \log g \lesssim 9.1$. These pulsating DA WDs (or ZZ Ceti stars; also known as DAVs) constitute the most populous class of pulsating WDs and exhibit multi-periodic luminosity variations up to 0.40 mag due to nonradial g(gravity)-mode pulsations of low harmonic degree ($\ell = 1, 2$) and periods between ∼70 s and ∼1500 s (see Winget & Kepler 2008; Althaus et al. 2010b; Córsico et al. 2019, for reviews).

Two main avenues are usually considered in asteroseismic modeling of pulsating WD stars. One approach assumes WD structures characterized by parameterized chemical composition profiles. This constitutes a powerful forward method that allows for a comprehensive exploration of the parameter space to infer an optimum asteroseismological solution (see Bradley 1998, 2001; Metcalfe et al. 2002; Bischoff-Kim et al. 2008, 2014, 2019; Castanheira & Kepler 2009; Fu et al. 2013; Bognár et al. 2016; Giammichele et al. 2017a,b, 2021, and references therein). The other approach, which relies on chemical profiles predicted by the complete evolutionary history of progenitor stars, is a grid-based approach developed by La Plata

Group and has been applied to GW Vir stars (pulsating PG 1159 stars; Córsico et al. 2008), V777 Her stars (pulsating helium(He)-rich atmospheres or DBVs; Córsico et al. 2012), ELMV stars (Calcaferro et al. 2017), and ZZ Ceti stars (Romero et al. 2012, hereinafter R12). The asteroseismological fits we carried out in R12 for 44 bright ZZ Ceti stars and subsequent works, such as Romero et al. (2013, 2017), are the first to be based on a grid of fully evolutionary ZZ Ceti models characterized by consistent chemical profiles from the center to the surface and covering a wide range of stellar masses, thicknesses of the H envelope and effective temperatures; more specifically, such studies have used the grid of DA WD models developed in Althaus et al. (2010a) and Renedo et al. (2010). One of the main emphases of such models is the evolutionary history of WD progenitors, since the internal chemical stratification of WDs is the result of numerous processes that take place during progenitor evolution – basically core He burning and convective boundary mixing during this stage, and the whole Asymptotic Giant Branch (AGB) and thermally pulsing AGB (TP-AGB) phases. The impact of these processes on the pulsational properties of WDs has recently been shown to be important and should be taken into account in detailed asteroseismological analysis of pulsating WDs (De Gerónimo et al. 2017, 2018).

Uninterrupted observations from current and future space missions such as TESS (Ricker et al. 2015), Cheops (Moya et al. 2018), and PLATO (Piotto 2018), together with the *Gaia* (Gaia Collaboration 2016) data, are expected to dramatically increase the number of ZZ Ceti stars (see Romero et al. 2022), providing unprecedented high-quality observations (Córsico 2020, 2022). The interpretation of these data demands the development of a new generation of fully evolutionary ZZ Ceti models. In this paper, we present a new grid of WD models that are appropriate for conducting future asteroseismological studies of ZZ Ceti stars, with the main emphasis on the impact of their chemical profiles on the Brunt–Väisälä frequency and pulsational adiabatic periods. This new grid of WD models constitutes a major improvement over the ZZ Ceti models developed by Althaus et al. (2010a) and Renedo et al. (2010) used in the asteroseismological fits in R12. Specifically, we concentrate on generating WD stellar models with masses in the range of ∼0.52 to ∼0.83 $M_{\odot}$, resulting from the whole evolution of initially 1.5–4.0 $M_{\odot}$ mass star models, which embraces the range of stellar masses expected for most of the observed ZZ Ceti stars. The new grid presented here takes into account the advances in the last decade in the modeling and input physics of both the progenitor and WD stars that will be necessary to exploit the potential of the incoming observations of ZZ Ceti stars.

The paper is organized as follows. In Sect. 2, we describe the major improvements of our new grid of models over that used in R12. In Sect. 3, we describe the consequences for the pulsational properties of ZZ Ceti stars. Finally, in Sect. 4, we summarize the main findings of the paper.

2. New WD evolutionary models

The new models presented here avoid several shortcomings that are present in the set of evolutionary ZZ Ceti models developed in Althaus et al. (2010a). This set has constituted the base for the asteroseismological fits we carried out in R12 and subsequent works. More importantly, the new models take into account new advances in the modeling and input physics of both the progenitor and WD stars that will be of utmost importance for future asteroseismological inferences of WDs.

The new set of WD models uses as an input the complete evolution of progenitor stars evolved from the main sequence through the TP-AGB phase, by employing a recently updated version of our stellar evolution code LPCODE developed by La Plata group. LPCODE provides WD models characterized by consistent chemical profiles for both the core and envelope as a result of the full computation of the evolution of progenitor stars. This code has been widely used and tested in numerous stellar evolution contexts of low-mass and WD stars (see Althaus et al. 2003, 2005, 2015; Salaris et al. 2013; Miller Bertolami 2016; Silva Aguirre et al. 2020; Christensen-Dalsgaard et al. 2020, for details). In particular, and relevant for this work, LPCODE computes WD evolution in a self-consistent way with the changes in the internal chemical distribution that result from the mixing of all the core chemical components induced by mean molecular weight inversions left by prior evolution, element diffusion, and convective mixing. Also, residual nuclear burning down to advanced evolutionary stages of WD evolution is allowed. The role played by residual H burning is not negligible (see Chen et al. 2021, for recent observational evidence of quiescent thermonuclear activity occurring in cooling WDs) and by the time evolution reaches the ZZ Ceti domain, it has yielded a substantial reduction of the H content with which the WD enters its cooling branch.

2.1. Improvements of the new models compared to our previous ones

We highlight below the improvements of our new set of models over those presented in Althaus et al. (2010a) that are expected to impact the period spectrum of ZZ Ceti stars:

Thickness of H envelope. The range of the H envelope has been extended to $\log(M_{\rm H}/M_{\odot}) = -13.5$, in contrast to the lowest H content we adopted in R12 of $\log(M_{\rm H}/M_{\odot}) = -9.5$. This will allow for seismological solutions for ZZ Ceti stars with extremely thin H envelopes to be found (if, indeed, they exist). This was not possible in R12. To this end, we artificially reduced the H content of our post-AGB sequences, so as to mimic a more efficient H mixing to deeper layers and burning expected during a very late thermal pulse (VLTP) episode in a possible single evolution scenario that predicts the formation of H-poor WDs, (see Córsico et al. 2019, for a recent discussion). As a result of this procedure, only tiny vestiges of H remain, extending from the surface down to deeper layers. As the WD cools down, such traces of H float to the surface as a result of gravitational settling, thus forming an increasing pure (and thin) H envelope. To properly follow this process, LPCODE considers a new fully implicit treatment of time-dependent element diffusion that includes thermal, chemical diffusion, gravitational settling (Althaus et al. 2020b), and Coulomb diffusion (see below). We follow the diffusion of the isotopes ^{1}H,^{3}He, ^{4}He, ^{12}C, ^{13}C, ^{14}N,^{15}N, ^{16}O, ^{17}O,^{18}O, ^{19}F, ^{20}Ne, and ^{22}Ne.

Treatment of core He burning. The new set of models presented here are based on a more realistic implementation of convective boundary mixing toward the end of He-core burning (Miller Bertolami 2016) than what we performed in R12. This yields a larger central oxygen (O) abundance for the same initial mass $M_{\rm i}$ and a very abrupt variation of the abundances of O and carbon (C) in the core.

^{22}Ne diffusion. Due to the two neutron excess of ^{22}Ne, this isotope rapidly sediments in the interior of WDs (Bravo et al. 1992), thus releasing an additional amount of

Table 1. Main characteristics of our progenitor and WD sequences.

$M_{\rm i}$ $[M_\odot]$	$M_{\rm WD}$ $[M_\odot]$	HeCF	$\tau_{\rm pre\text{-}WD}$ [Myr]	$M_{\rm c}^{\rm 1TP}$ $[M_\odot]$	$\log M_{\rm H}$ $[M_\odot]$	$\log M_{\rm H}^{\rm ZZ}$ $[M_\odot]$	$N_{\rm C}/N_{\rm O}$
1.00	0.5281	Yes	11 813	0.5119	−3.60	−3.93	0.40
1.25	0.5614	Yes	5256.6	0.5268	−3.77	−4.04	0.37
1.50	0.5759	Yes	2820.6	0.5267	−3.93	−4.28	2.20
2.00	0.5803	No	1418.9	0.4873	−4.11	−4.23	1.12
3.00	0.6573	No	442.92	0.6103	−4.47	−4.59	1.66
4.00	0.8328	No	195.90	0.8086	−5.17	−5.32	0.81

Notes. $M_{\rm i}$: Initial mass of the model (at ZAMS). $M_{\rm WD}$: final WD mass. HeCF: Full He-core flash at the beginning of the core He-burning phase. $\tau_{\rm pre\text{-}WDMS}$: Lifetime from the ZAMS to the onset of WD cooling branch. $M_{\rm c}^{\rm 1TP}$: mass of the H-free core at the first thermal pulse (defined as those regions with $X_{\rm H} < 10^{-4}$). $M_{\rm H}$: Mass of the H content at the maximum effective temperature at the beginning of the WD cooling branch. $M_{\rm H}^{\rm ZZ}$: mass of the H content at the ZZ Ceti instability strip. $N_{\rm C}/N_{\rm O}$: C/O ratio as a number fraction at the end of the TP-AGB phase.

energy that delays the cooling times (Deloye & Bildsten 2002; Althaus et al. 2010c; García-Berro et al. 2010). More recently, Camisassa et al. (2016) explored the impact of ^{22}Ne sedimentation on the adiabatic pulsational properties of ZZ Ceti models and found that this process induces appreciable changes in the pulsation periods of ZZ Ceti stars (in the range between 10 s and 50 s depending on the stellar mass), which have to be taken into account in attempts to perform precise asteroseismology of these stars. A similar conclusion was recently presented in Chidester et al. (2021) in the case of DBV variable stars. These authors found the presence of a systematic offset in the periods of pulsating WD when ^{22}Ne diffusion is absent. In our new set of WD models, ^{22}Ne diffusion has been considered based on initial realistic ^{22}Ne abundances in the WD interior, resulting from the full evolution of solar metallicity progenitor stars. This constitutes a major improvement over our seismological models employed in R12, particularly in the case of more massive WDs.

Coulomb sedimentation. Another piece of WD physics that was neglected in R12 was the separation of ions due to Coulomb interactions at high densities. This process affects the diffusion flux in WDs (Beznogov & Yakovlev 2013; Chang et al. 2010), driving the gravitational settling of ions with the same mass to charge number A/Z, as in the case of plasmas rich in ^{4}He and ^{12}C. Recently, Althaus et al. (2020a) showed that, in the case of massive WDs, Coulomb separation produces marked changes in the g-mode pulsation periods (up to ∼15%) that cannot be neglected in detailed asteroseismological analyses of ZZ Ceti stars. Coulomb sedimentation has been incorporated in a time-dependent diffusion treatment, as given in Althaus et al. (2020a).

Progenitor evolution. The evolutionary history of progenitor star determines the internal chemical profile of the WD and, hence, the pulsational properties of ZZ Ceti stars. The starting configurations for our new set of WD models are the H-burning post-AGB star models with metallicity $Z = 0.02$ derived by Miller Bertolami (2016), who considered new observational constraints and recent advances in the micro- and macro-physics involved in the core He burning in AGB and TP-AGB modeling. Among these improvements, we note the inclusion of updated low-temperature opacities for the C- and O-rich AGB stars, a consistent treatment of the stellar winds for the C- and O-rich regimes, and an updated and improved description of convective boundary mixing processes during the thermal pulses and previous evolutionary stages[1]. These improvements have led to stellar models characterized by the occurrence of appreciable third dredge-up (3DUP) and C enrichment of the envelope that reproduce many relevant AGB and post-AGB observables, in particular the C/O ratios of AGB and post-AGB stars in the Galactic disk, the WD initial-final mass relation (IFMR) at near solar metallicities, the C–O intershell abundances of AGB stars as observed in PG1159 stars, and the mass range of C-rich stars in the stellar clusters of the Magellanic Clouds. In addition, the properties of the resulting AGB stellar models such as core growth, C enrichment, and IFMR are well in agreement with the predictions of modern AGB grids, so the predicted structures can be considered good representatives of state-of-the-art AGB stellar evolution modeling for the post-AGB phase (see Miller Bertolami 2016, for details). The 3DUP episodes, which are strongly inhibited in progenitor stars of the ZZ Ceti models used in R12, alter the IFMR and thus impact the core chemical composition and the envelope structure of a WD of given mass (see Althaus et al. 2010a). The H-burning post-AGB sequences of Miller Bertolami (2016) also reproduce the observed range of He-, C-, and O-intershell abundances of AGB stars, as determined from the observations of PG1159 stars (see Werner & Herwig 2006). This is of utmost importance for the envelope chemical stratification of ZZ Ceti stars and their pulsational properties (Althaus et al. 2010a). In addition, the 3DUP episodes lead to the formation of WDs with less massive H envelopes and pockets of abundant ^{13}C and ^{14}N. Finally, the agreement with observational data of the C/O ratio of PNe shows that the new models depart from the TP-AGB at the right time in terms of C enrichment, thus lending confidence to the accuracy of the thermochemical structure of our WD models (see Miller Bertolami 2016).

Table 1 summarizes some characteristics of progenitor stars of our new ZZ Ceti models that are relevant for the WD formation. The initial mass ($M_{\rm i}$) of progenitor stars at the ZAMS ranges from 1.5 to 4.0 $M_\odot$, which yield final WD masses ($M_{\rm WD}$) in the range from 0.5281 to 0.8328 $M_\odot$. Some features deserve some additional commentary. We note that the 1.5–2.0 $M_\odot$ progenitors lead to quite similar WD masses, inflicting a pronounced plateau in the IFMR at that range of masses. This is connected with the transition from degenerate to nondegenerate He-core ignition at that range of initial masses and the resulting different sizes of the H-free core during He-core burning. This also explains the minimum in the H-free core mass at the first thermal pulse (see Col. (5) in Table 1 at $M_{\rm i} \approx 2\,M_\odot$).

Most of our sequences experience efficient 3DUP episodes and C enrichment of the envelope, with the exception of the lower-mass models. As a result, most of our models become

[1] Convective boundary mixing during the thermal pulses was disregarded in the computation of progenitor stars of the ZZ Ceti models used in R12.

C-rich during the TP-AGB evolution, namely, $N_C/N_O > 1$ (see Col. (8) in Table 1), which is in agreement with the expected C enrichment as observed in many AGB and post-AGB stars (see Miller Bertolami 2016). The high C/O ratio that characterizes our $M_i = 1.5\,M_\odot$ model results from the fact that this model underwent a final thermal pulse shortly after the end of the TP-AGB. As a result, the C dredged up to the surface is diluted into a significantly smaller mass of H, leading to a higher surface C abundance. The occurrence of 3DUP is key in determining the IFMR. Intense 3DUP delays the growth of the H-free core during the TP-AGB evolution, yielding smaller final WD masses than in the absence of 3DUP for the same initial mass M_i. As mentioned above, this is relevant for the internal chemical composition of a WD of given mass. In addition, the higher C enrichment of the envelope resulting from efficient 3DUP leads to smaller masses of the H envelope at the departure from the AGB. An updated treatment of the previous evolution, related in particular to opacities and nuclear reaction rates, also leads to models that depart from the AGB with smaller H-envelope masses and brighter luminosities (see Miller Bertolami 2016 for details). The masses of the H content listed in Table 1 (Col. (6)) are upper limits for the maximum H content expected from our single progenitors at the onset of the cooling branch. By the time the domain of the ZZ Ceti stars is reached, the H content has been markedly reduced by residual H burning (see Col. (7) in Table 1).

2.2. Implications for the chemical profiles

The initial WD configurations provided by our new H-burning post-AGB models have evolved from the planetary nebulae stages down to the domain of the ZZ Ceti stars in a consistent way with abundance changes resulting from element diffusion, convective mixing, and residual nuclear burning. At high effective temperatures, we performed the core mixing implied by the inversion of the mean molecular weight left by prior evolution. The resulting chemical stratification for some selected isotopes by the time the evolution reached the ZZ Ceti domain, at $T_{\rm eff} \sim 12\,000$ K, is displayed in Fig. 1 for the 0.5281, 0.5759, 0.6573, and 0.8328 $M_\odot$ WD models; it is also compared with the chemical stratification of ZZ Ceti models used in R12 of similar stellar masses (thick and thin lines, respectively).

Clearly, the new H-burning post-AGB models predict chemical structures for the ZZ Ceti stars substantially different from those characterizing the R12 models. The internal composition of WDs is a crucial aspect for the determination of the pulsational properties of these stars. The impact of these new chemical structures on the theoretical pulsational spectrum of ZZ Ceti stars should hence be assessed. Three main improvements in the treatment of progenitor evolution of our new ZZ Ceti models, which have a direct impact on the WD chemical profile, can be identified. First, as mentioned, the more careful implementation of convective boundary mixing toward the end of He-core burning performed in Miller Bertolami (2016), which yields a larger central O abundance for the same initial mass M_i. This feature implies a very abrupt variation of the abundances of O and C in the core and, as we show later in this work (Sect. 3), this has a dramatic impact on the pulsational properties of our new models. Second, the occurrence of appreciable 3DUP during the TP-AGB phase in our progenitor stars, which leads to smaller WD masses, particularly in the case of intermediate-mass stars. In particular, our new progenitor treatment predicts an initial mass of $M_i = 3\,M_\odot$ for the $0.6573\,M_\odot$ WD model, while the same WD mass corresponds to a $M_i = 2.5\,M_\odot$ progenitor star in the set of ZZ Ceti models used in R12. This explains the smaller central O abundance we find for this WD model, as compared with that of R12[2]. Third, the evolutionary history of WD progenitors includes the possibility that they may experience the last thermal pulse shortly after departing from the TP-AGB. This is relevant concerning the location in mass of the He-rich buffer and the underlying intershell region rich in He and C build up by the He-flash convection zone at the last AGB thermal pulse. This is particularly clear in the $0.5759\,M_\odot$ WD model resulting from the $M_i = 1.5\,M_\odot$ progenitor that undergoes a late thermal pulse. We note in this case that both the location and chemical profile of the intershell region result markedly affected by the occurrence of a late thermal pulse. The presence of C in the intershell region stems from the mixing due to the short-lived He-flash convection zone that pushed the C-rich zone upward during the peak

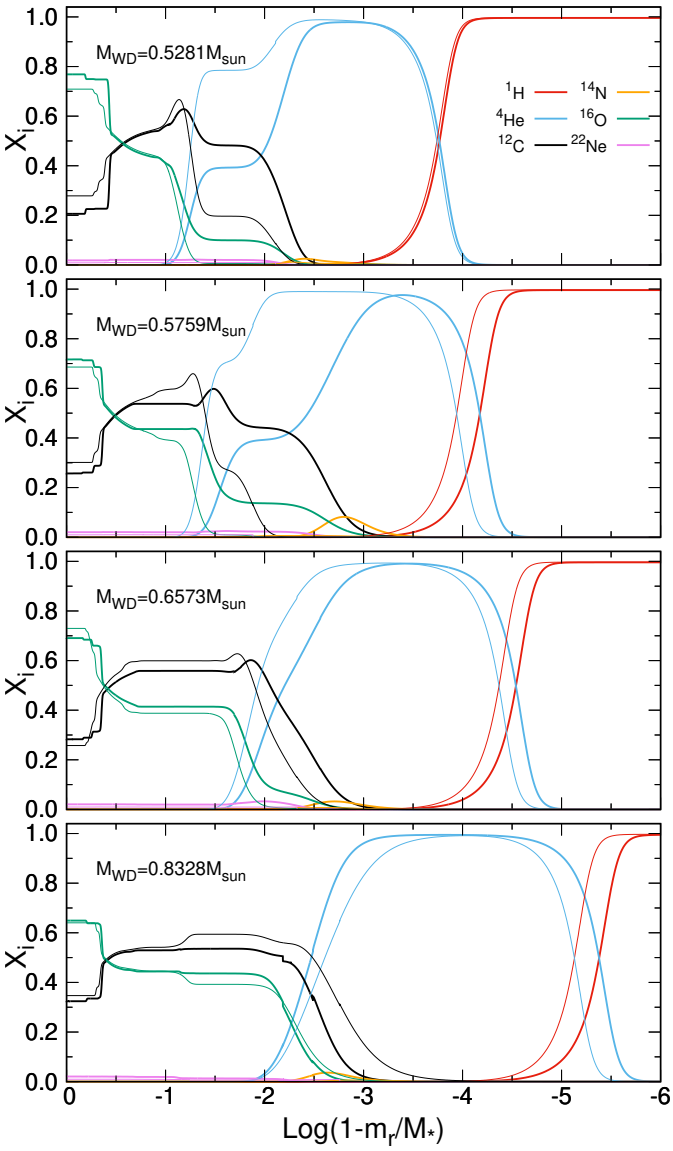

Fig. 1. Abundance by mass of ^{1}H, ^{4}He, ^{12}C, ^{14}N, ^{16}O, and ^{22}Ne in terms of the outer mass coordinate for our 0.5281, 0.5759, 0.6573, and 0.8328 $M_\odot$ WD models at the domain of the pulsating ZZ Ceti stars. Our new chemical profiles are compared with those we used in R12 of similar stellar masses (thick and thin lines, respectively).

[2] At this range of M_i, the central O abundance decreases with increasing M_i.

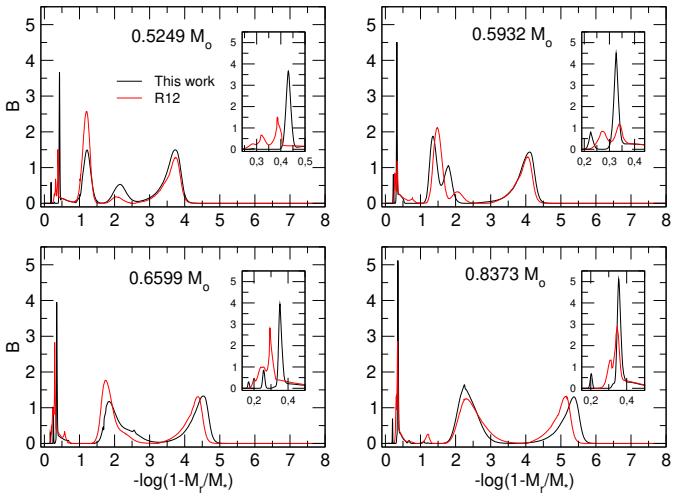

Fig. 2. Ledoux term B in terms of the outer mass fraction as predicted by our DA WD template models with different masses and a thick H envelope and by those used in R12 (black and red lines, respectively). The various features exhibited by B can be directly related to the different chemical transition regions of the models (see Fig. 1). In each panel, the inset is a zoom of the C/O-core region.

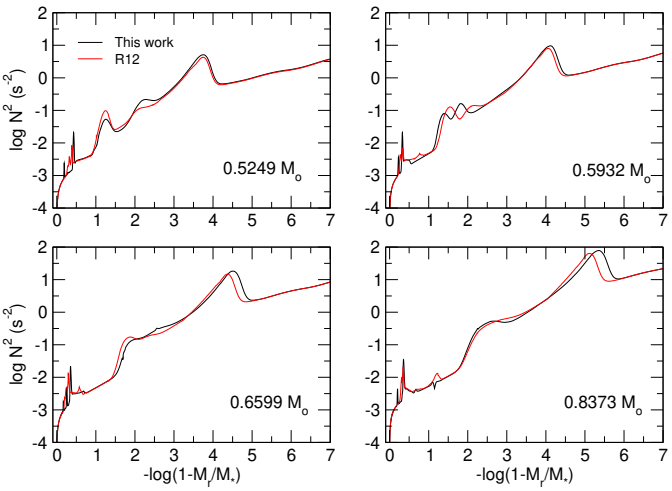

Fig. 3. Brunt–Väisälä frequency in terms of the outer mass fraction corresponding to our DA WD template models with different masses and a thick H envelope and by those employed in R12 (black and red lines, respectively).

of the last He thermal pulse in the AGB. Because of the inclusion of convective boundary mixing during the TP-AGB in our new sequences, particularly at the pulse-driven convection zone, a larger O abundance is predicted in the intershell region. Also, the large abundance of ^{14}N in the He-rich buffer (in particular for the 0.5759 $M_\odot$ ZZ Ceti model) is due to the occurrence of appreciable 3DUP in its progenitor star and the subsequent H burning in a C-enriched medium. We also note that the more efficient 3DUP experienced by our progenitor stars leads to maximum masses of the H content that are markedly smaller than those characterizing the set of ZZ Ceti models of R12 and described in Althaus et al. (2010a) and Renedo et al. (2010). This is not the case for the 0.5281 $M_\odot$ ZZ Ceti model, the progenitor of which avoids the C enrichment of the envelope (see Table 1), resulting in a final H content similar to that of Renedo et al. (2010). Finally, for both sets of ZZ Ceti models, the H and He contents left by progenitor evolution decrease with WD mass.

During WD cooling, element diffusion processes modify the chemical abundance distribution in the outer layers left by prior mixing and burning episodes during the TP-AGB evolution. This is more noticeable in the case of more massive WDs, for which the inter-shell rich in He, C, and O is completed eroded by chemical diffusion by the time the domain of the ZZ Ceti stars is reached. For the least massive WD model, we note that such an intershell region is still present at this stage. The presence of such double-layered structure affects the pulsational periods of ZZ Ceti stars (see Althaus et al. 2010a). In the more massive models, chemical diffusion is also responsible for the presence of abundant C in the He-buffer zone. Another improvement in our new ZZ Ceti models which (as noted above) impacts the predicted pulsation periods of ZZ Ceti stars, is ^{22}Ne diffusion. Here, the abrupt change in the initial ^{22}Ne profile at the edge of the CO core is strongly smoothed out by diffusion, leading to the formation of a bump in its abundance. Finally, the chemical profiles shown in Fig. 1 bear the signature of Coulomb sedimentation. This process is relevant for the more massive WDs and for mixtures of ions with equal A/Z. In this case, Coulomb separation drives gravitational settling and ions with larger Z move to deeper layers. We note that the H–He interface is not affected by Coulomb diffusion because in this case the contribution due to gravity is dominant, and Coulomb diffusion represents a minor contribution to the diffusion flux. Both ^{22}Ne diffusion and Coulomb sedimentation were not considered in the set of ZZ Ceti models employed in R12.

3. Impact on the pulsational properties of ZZ Ceti stars

In this section, we compare the pulsational properties of our new ZZ Ceti models with those of R12. This comparison is of utmost relevance, given that the R12 DA WDs models have also been generated with the LPCODE – with an earlier version, however – and they are currently being used in the grid-based asteroseismological approach with fully evolutionary stellar models. Because the models of R12 and those that we present in this paper primarily differ in terms of the internal chemical structure, we can anticipate that there will be appreciable differences in the oscillation periods and the period spacings of the g modes. We emphasize that the differences in the chemical profiles of our models as compared with the R12 ones are the result of the integrated effects of the incorporation of Ne diffusion, the inclusion of Coulomb sedimentation, the different treatment of core He burning, and the distinct progenitor evolution modeling. That said, here we do not seek to examine the individual effect of each of these ingredients of our modeling, since this has been done to a great extent in other works (Camisassa et al. 2016; Chidester et al. 2021; Althaus et al. 2020a). Rather, we examine models with the same stellar mass and effective temperature, along with very similar thicknesses of the H envelope, in order to assess the changes in the periods and the period spacings introduced by the employment of our new evolutionary models.

The pulsation modes of our new ZZ Ceti models as well as those of the R12 models have been computed with the same adiabatic version of the LP-PUL pulsation code described in Córsico & Althaus (2006). The squared Brunt–Väisälä frequency (N, the critical frequency of nonradial g-mode pulsations) is computed as in Tassoul et al. (1990), according to the following expression:

$$N^2 = \frac{g^2\rho}{P}\frac{\chi_T}{\chi_\rho}\,[\nabla_{ad} - \nabla + B], \qquad (1)$$

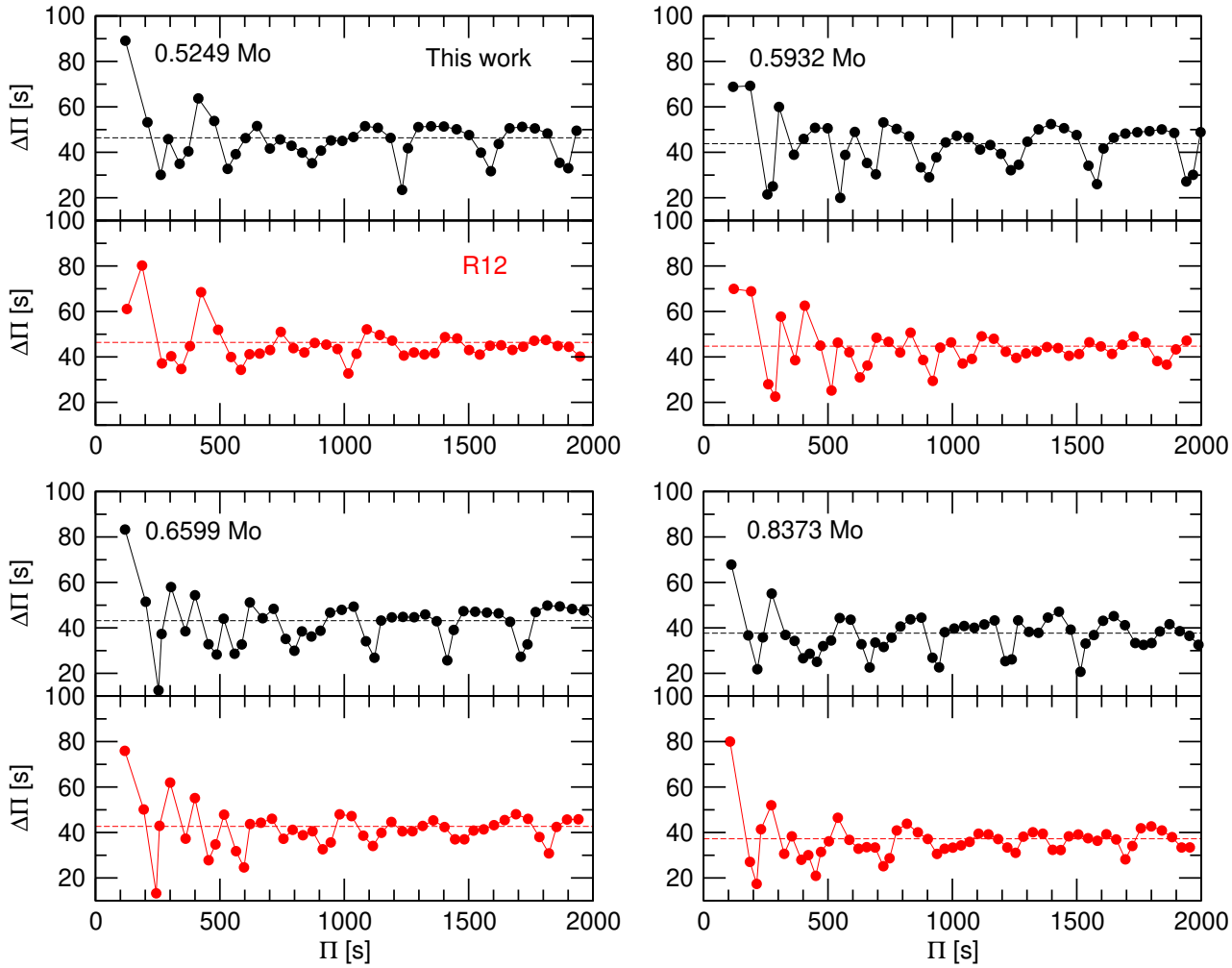

Fig. 4. Dipole ($\ell = 1$) forward period spacing versus periods for our template DA WD models with thick H envelopes, say $\log(M_{\rm H}/M_\star)$ between -4 and -5, and for the models of R12 with similar H thicknesses (black dots and red dots, respectively). The asymptotic period spacing for both sets of models is plotted with dashed lines.

where g, ρ, P, $\nabla_{\rm ad}$, and ∇ are the acceleration of gravity, density, pressure, adiabatic temperature gradient, and actual temperature gradient, respectively. The compressibilities are defined as:

$$\chi_\rho = \left(\frac{{\rm d}\ln P}{{\rm d}\ln\rho}\right)_{\rm T,\{X_i\}} \quad \chi_{\rm T} = \left(\frac{{\rm d}\ln P}{{\rm d}\ln T}\right)_{\rho,\{\rm X_i\}}. \tag{2}$$

Finally, the Ledoux term B is computed as (Tassoul et al. 1990):

$$B = -\frac{1}{\chi_{\rm T}}\sum_{1}^{M-1}\chi_{\rm X_i}\frac{{\rm d}\ln X_i}{{\rm d}\ln P}, \tag{3}$$

where

$$\chi_{\rm X_i} = \left(\frac{{\rm d}\ln P}{{\rm d}\ln X_i}\right)_{\rho,\rm T,\{X_{j\neq i}\}}. \tag{4}$$

The computation of the Ledoux term includes the effects of an arbitrary number of chemical species that vary in abundance in the transition regions. In the following sections, we first focus on examining DA WD models with canonical H envelopes, that is, the thickest possible H envelopes according to our detailed pre-WD evolutionary calculations. Then, we focus on models with thin H envelopes. Finally, we focus on the pulsation properties of models with ultra-thin H envelopes.

3.1. DA WDs with thick H envelopes

We considered the following values of the stellar mass: 0.5249, 0.5932, 0.6599, and 0.8373 $M_\odot$, in agreement with some sequences of the R12 computations (their Table 1). We picked four template models of our set of structures with effective temperature ∼12 000 K and canonical (thick) H envelopes, $\log(M_{\rm H}/M_\star) \sim -4$ to -5. These models have been derived from interpolation from our set of models listed in Table 1. We emphasize that in order to isolate as much as possible the effects of the differences in the chemical profiles on the pulsation periods, we adopted stellar mass values that are exactly equal to those considered by R12. In Fig. 2, we show the Ledoux term B versus the logarithm of the outer mass fraction for the template models, where we use red curves for the R12 models. The insets of each panel amplify the region of the CO core. We find that the peaks associated with the O/C/He and He/H transition regions of our set of models are similar to those of the R12 models, although in some cases (0.5249 $M_\odot$ and 0.6599 $M_\odot$), the peak due to the triple transition (O/C/He) is more important in the case of R12 models. The strongest differences in B, however, come from the contribution of the O/C chemical interface, which is much more noticeable in the models of the present work for all the examined stellar masses. In particular, for the case of $M_\star = 0.5932\,M_\odot$, the peak of the Ledoux term of our template model is more than

four times higher than for the analogous model of R12. This is due to the much more abrupt step of the O and C chemical abundances in the core of our models (see Fig. 1), which makes the contribution to B much more noticeable in the models presented in this paper than in the models of R12. The run of the squared Brunt–Väisälä frequency for the same models is shown in Fig. 3. Although the Brunt–Väisälä frequencies are almost similar in both sets of models, the peaks corresponding to the CO-core chemical transition are more pronounced in the new models.

The differences in B and $\log(N^2)$ described above have dramatic consequences for the mode-trapping characteristics of our new models. This is revealed by plotting the forward period spacing ($\Delta\Pi = \Pi_{k+1} - \Pi_k$) versus the periods, as shown in Fig. 4. It is clear from the figure that for periods of up to ∼900−1000 s, the period spacing of both sets of models looks qualitatively similar, showing small differences for a few modes. However, for longer periods, the period spacing of our new models exhibits strong minima, even for very long periods ($\gtrsim$2000 s, not plotted), while the R12 models exhibit mode-trapping features with decreasing amplitudes and with period spacings gradually closer to the constant asymptotic limit (horizontal dotted lines), as we considered longer and longer periods.

To find the reason for the occurrence of these minima in our models, we recalculated the full spectrum of periods by forcing the Ledoux term B to be zero locally at the different chemical transition regions to estimate the impact that each single interface has on the mode-trapping properties (see, for instance, Brassard et al. 1992; Córsico & Althaus 2005). This simple exercise reveals that the strong minima in $\Delta\Pi$ for periods longer than ∼900−1000 s in our new models are due to the presence of the very sharp peak in N near the stellar centre, which originates from the abrupt step of the chemical composition profile in the core region. This feature is absent in the R12 models. We show in Fig. 5 the chemical profile of O (upper panel) at the O/C interface for a model with $M_\star = 0.5932\,M_\odot$ and $T_{\rm eff} \sim 12\,000$ K in the case of the present model computations and in the case of the R12 model set. The difference in the slope of the drop in the O abundance for our model and that of the R12 models is very noticeable (see around $\log(1 - M_r/M_\star) \sim -0.32$). We also show the Ledoux term B at the region of the O/C interface of our model (middle panel), $B_{\rm OC}$, along with the situations in which we assume $B_{\rm OC}/2$, $B_{\rm OC}/4$, and the extreme case in which $B_{\rm OC} = 0$. Finally, we show the logarithm of the squared Brunt–Väisälä frequency (lower panel) for the same cases considered in the middle panel. In Fig. 6, we display the period spacing for the same models considered in Fig. 5. As we artificially reduce the magnitude of the Ledoux term, the contribution of the O/C interface becomes less and less important, until it is negligible in the most extreme case in which $B_{\rm OC} = 0$. In parallel, the very pronounced minima in the period spacings (left panel) become less pronounced, until they almost disappear when $B_{\rm OC} = 0$. We note that the minima of $\Delta\Pi$ correspond to local maxima in oscillation kinetic-energy distribution, as depicted in the right panel. This reveals that these modes have finite amplitudes of oscillation in central regions, where the density is high, and therefore they are characterized by large kinetic energies. These modes can be considered as modes partially "confined" to the core of the star. We conclude that the pronounced minima in $\Delta\Pi$ for periods longer than ∼900−1000 s are produced by the sharp structure of the O/C transition zone of the core. On the other hand, the mode-trapping features for periods shorter than ∼900−1000 s are inflicted mainly by the He/H transition region and, to a lesser extent, by the O/C/He interface. This is valid for both sets of models. We conclude that the mode-trapping characteristics of our models and those of R12, in both cases with thick H envelopes, are qualitatively similar to each other for short periods, but they differ significantly for longer periods.

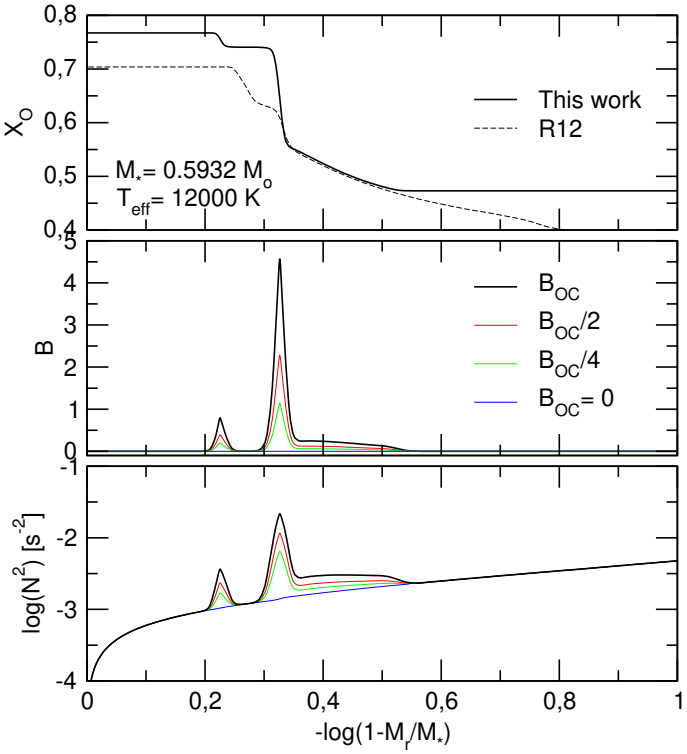

Fig. 5. Main differences in the properties of the core of the models between the present calculations and those of R12. *Upper panel*: chemical profile of O at the CO-core regions of a DA WD model with $M_\star = 0.5932\,M_\odot$, $T_{\rm eff} \sim 12\,000$ K, and a thick H envelope, for the case of the present calculations (solid black line) and the R12 computations (dashed black line). *Middle panel*: Ledoux term B at the region of the O/C interface, $B_{\rm OC}$, of the same model depicted in the *upper panel*, along with the artificial situations of $B_{\rm OC}/2$, $B_{\rm OC}/4$, and $B_{\rm OC} = 0$. *Lower panel*: logarithm of the squared Brunt–Väisälä frequency for the same cases considered in the middle panel.

In closing this section, we quantitatively assess the differences in the individual periods between our models and those of R12. In Fig. 7 we show the difference $\delta\Pi_k = \Pi_k - \Pi_{k,\rm R12}$ versus the radial order (k) for the models examined in the previous figures. Clearly, there are very important differences (of up to ∼45 s) in excess or in defect in the pulsation periods of g modes with the same k, except for the case of low-order modes, for which the differences are lower, but still important (∼20 s). The differences found in the periods and in the period spacings considering our new set of DA WD models have their origin in the various improvements in the treatments of different physical processes during the evolution of the progenitors (for instance, the treatment of core helium burning) and as well as along the evolution of the WD stage (such as incorporating Ne diffusion and Coulomb sedimentation). This is an important result that suggests that there would be substantial differences in the asteroseismological determinations of ZZ Ceti stars with thick H envelopes depending on whether the old R12 models or the new models presented in this work are employed. This important issue will be addressed in subsequent papers (Córsico & Althaus, in prep.).

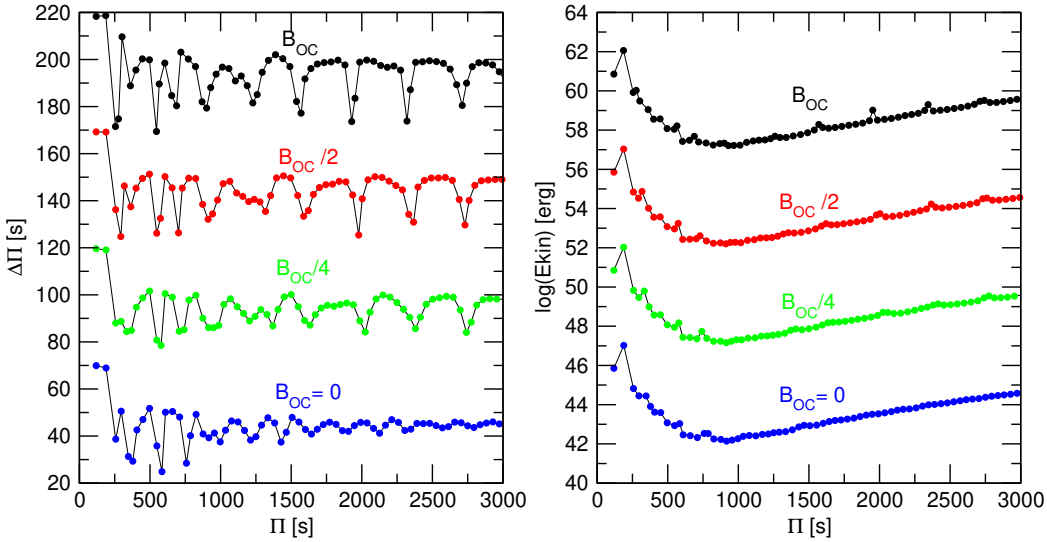

Fig. 6. The impact of the CO chemical transition at the core on the distribution of period spacings and kinetic energies of oscillation of the new models. *Left panel*: $\ell = 1$ forward period spacing $\Delta\Pi$ in terms of the pulsation periods, for a decreasing magnitude of Ledoux term B at the CO chemical interface ($B_{\rm OC}$), from the *top to the bottom panel*. The curves have been artificially displaced up for clarity, where y-axis values make sense only for the case $B_{\rm OC} = 0$. *Right panel*: similar to the left panel, but for the oscillation kinetic energy. The models have $T_{\rm eff} \sim 12\,000$ K, $M_\star = 0.5932\,M_\odot$, and thick H envelopes.

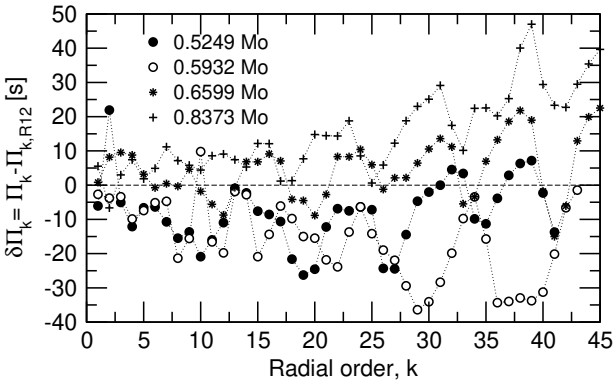

Fig. 7. Differences between the $\ell = 1$ pulsation periods of our template DA WD models with thick H envelope and the periods corresponding to the R12 models, in terms of the radial order, for different stellar masses.

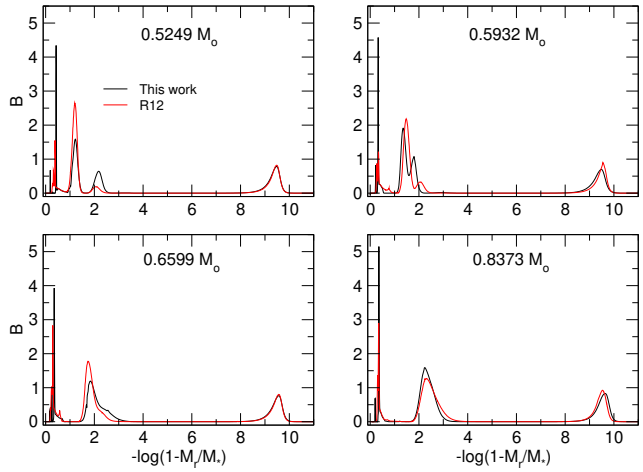

Fig. 8. Ledoux term B in terms of the outer mass fraction as predicted by our DA WD template models with different masses and a thin H envelope, and by those used in R12 (black and red lines, respectively).

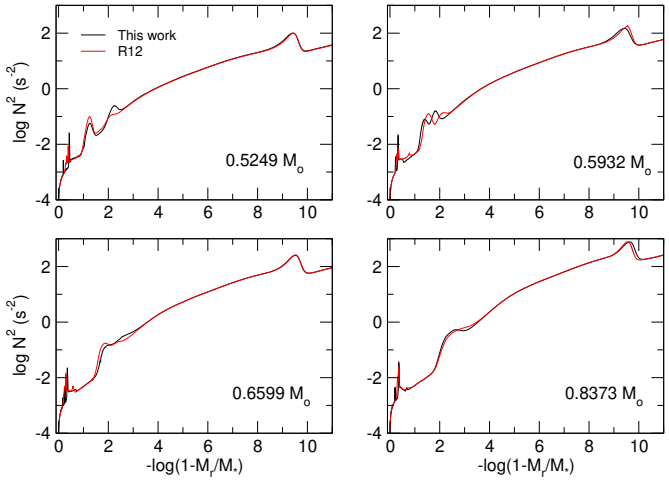

Fig. 9. Brunt–Väisälä frequency in terms of the outer mass fraction corresponding to our DA WD template models with different masses and a thin H envelope and by those employed in R12 (black and red lines, respectively).

3.2. DA WDs with thin H envelopes

We repeated the analysis of the previous section, this time by considering template DA WD models with thin H envelopes, $\log(M_{\rm H}/M_\star) \sim -9.3$. These envelopes are thinner by four orders of magnitude than those considered in the previous section. The asteroseismological analysis of R12 indicates that many ZZ Cetis could harbour H envelopes this thin, so this case is of utmost relevance. We show in Fig. 8 the Ledoux term B for our template models and for the models of R12, and in Fig. 9 the corresponding Brunt–Väisälä frequency profiles. Since the chemical structure of the core and the triple chemical transition regions do not change in comparison with the thick H envelope models discussed above, the only novel feature of these figures is the value of B at the He/H transition. We note that the value of B in this external chemical transition is almost identical in our

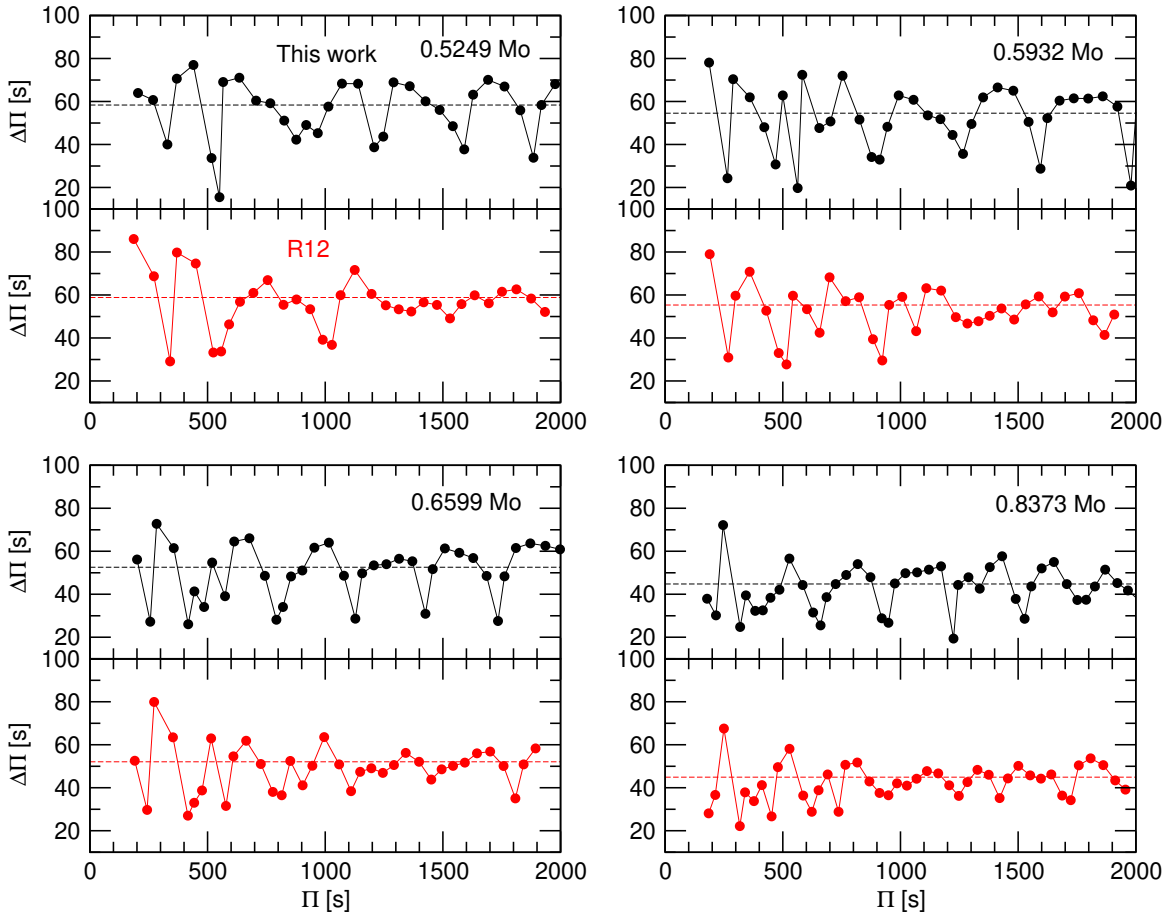

Fig. 10. Dipole ($\ell = 1$) forward period spacing versus periods for our template DA WD models with thin H envelopes, say $\log(M_{\rm H}/M_\star) = -9.3$, and for the models of R12 with similar H thicknesses (black dots and red dots, respectively). The asymptotic period spacing for both sets of models is plotted with dashed lines.

models and in the R12 models, and so is the contribution to the Brunt–Väisälä frequency. Therefore, the differences in the periods of both sets of models will come from the differences in the chemical structure of the core and the triple transition region. We display in Fig. 10 the period spacing $\Delta\Pi$ for the models with thin H envelope considered in Figs. 8 and 9. As in the case of thick H envelope models, we note that the period spacing is qualitatively similar for both sets of models for periods shorter than ∼900−1000 s, but that important differences appear for longer periods. Specifically, the R12 models show a gradual approach of $\Delta\Pi$ to the asymptotic period spacing, while the models presented in this work exhibit strong minima for increasing periods. We verified, as in the case of thick H envelopes (see previous section), that the presence of the very sharp peak in N near the stellar centre of our models is responsible for the strong minima in $\Delta\Pi$ for long periods. This is at variance with the R12 models. The He/H transition, on the other hand, plays a secondary role for long periods, although it has a strong impact on $\Delta\Pi$ for short and intermediate periods. This last property is also typical of the R12 models. To quantify the discrepancies in the individual periods between our models and those of R12, we depict in Fig. 11 the differences of our periods minus those of R12 for fixed radial order. We conclude that period differences among ∼20 s and ∼40 s that we find between both sets of calculations, could affect the asteroseismologically derived stellar parameters of ZZ Ceti stars – in particular, for long-period pulsators – even in the case of thin H envelopes.

3.3. DA WDs with ultra-thin H envelopes

Finally, we describe the pulsation properties of DA WD models with ultra-thin H envelopes, that is, $\log(M_{\rm H}/M_\star) \sim -13.5$. Since there are no DA WD models of R12 with such thin H envelopes[3], we are prevented from comparing our results with their computations. The comprehensive survey of DA WD models of Brassard et al. (1992) includes H envelopes as thin as $\log(M_{\rm H}/M_\star) \sim -14$. However, since those old models have cores made of pure C with no O, they are not directly comparable to ours, since these harbour C/O cores. We show in Fig. 12, the Ledoux term B and in Fig. 13, the logarithm of the squared Brunt–Väisälä frequency for template models with ultra-thin H envelopes. We note that for the model with $M_\star = 0.8373\ M_\odot$, the peak corresponding to the He/H interface is very sharp and high compared to the models of the other masses. This is because, for such a thin H envelope and for that stellar mass, a thin convective region appears in the He/H transition zone that mixes He and H, generating an abrupt step in the chemical profile that gives rise to that sharp peak in B. The resulting period-spacing diagrams are depicted in Fig. 14. These diagrams look very similar to the previous ones corresponding to thicker envelopes, namely, a pattern of minima and maxima more or less irregular, due to the impact of the He/H transition and the triple O/C/He transition, for periods shorter than ∼900−1000 s, and a quite regular pattern characterized by very deep minima due mainly to the chemical

[3] They reach, at most, up to $\log(M_{\rm H}/M_\star) \sim -9.3$.

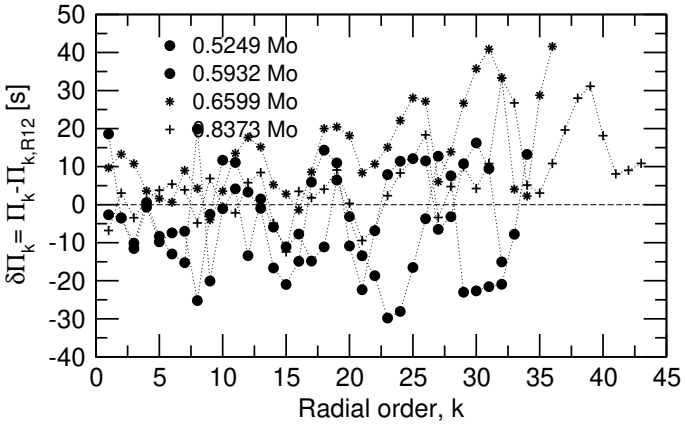

Fig. 11. Differences between the $\ell = 1$ pulsation periods of our template DA WD models with thin H envelope and the periods corresponding to the R12 models, in terms of the radial order, for different stellar masses.

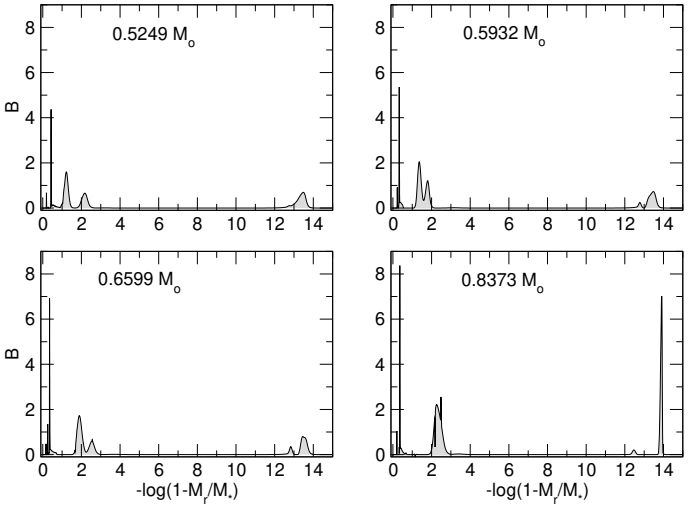

Fig. 12. Ledoux term B in terms of the outer mass fraction as predicted by our DA WD template models with different masses and a ultra-thin H envelope, that is $\log(M_{\rm H}/M_\star) \sim -13.4$.

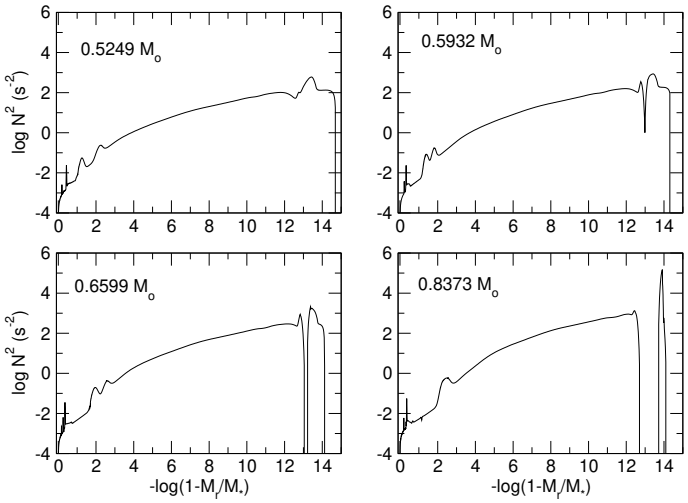

Fig. 13. Brunt–Väisälä frequency in terms of the outer mass fraction corresponding to our DA WD template models with different masses and a ultra-thin H envelope.

transition of the CO core, for periods longer than ∼900−1000 s. The inclusion of ultra-thin H envelopes in realistic models of DA WDs opens up for the first time the possibility of exploring the internal structure of ZZ Ceti stars with such thin H envelopes with asteroseismology.

4. Summary and conclusions

In this paper, we present a new grid of DA WD models appropriate for asteroseismology of ZZ Ceti stars that incorporates advances made over the last decade in the modeling and input physics of both the WD progenitors and WD stars. This new grid of models constitutes a major improvement over the ZZ Ceti models developed by Althaus et al. (2010a) and Renedo et al. (2010), which we made ample use of in numerous asteroseismological analyses like the study of R12 and subsequent works. Specifically, we generated DA WD stellar models with masses from ∼0.52 to ∼0.83 $M_\odot$, resulting from the whole evolution of initially 1.5–4.0 $M_\odot$ mass-star models, which embraces the range of stellar masses expected for most of the observed ZZ Ceti stars. Our models were derived in a self-consistent way with the changes in the internal chemical composition due to the mixing of core constituents induced by mean molecular weight inversions, ^{22}Ne diffusion, Coulomb sedimentation, and residual nuclear burning. Our new models also accounts for nuclear burning history and mixing events along the progenitor evolution, in particular the occurrence of third dredge-up, which determine the properties of the core and envelope of post-AGB and WD stars, as well as the WD initial-final mass relation. The range of H envelope thickness of our models extends from the maximun residual H content predicted by progenitor history, $\log(M_{\rm H}/M_\odot) \sim -4$ to -5, to $\log(M_{\rm H}/M_\odot) = -13.5$, thus allowing for the first models that permit (in the short term) for seismological solutions for ZZ Ceti stars with extremely thin H envelopes to be obtained – if, indeed, they do exist in nature. Calculations were performed with the LPCODE stellar evolution code.

Our new H-burning post-AGB models predict chemical structures for the ZZ Ceti stars substantially different from those used in seismological studies by R12. We discussed the implication of these new models for the pulsational spectrum of ZZ Ceti stars. We find that the pulsation periods of g modes and mode trapping properties of our new models differ significantly from those characterizing R12's ZZ Ceti models. Specifically, our new models are characterized by a very abrupt step in the C and O abundances at the stellar core, which have a dramatic impact on the pulsation periods themselves and also on the mode-trapping properties and consequently the period spacing. In the case of the period spacing, our models and those of R12 agree quite well for periods shorter than ∼900−1000 s, but strongly differ for longer periods. Specifically, for high radial-order modes ($\Pi \gtrsim 900-1000$ s), our models show a distribution of period spacings characterized by very pronounced minima, related to high oscillation-energy modes that have finite amplitudes in the CO-core regions. Instead, the period spacing of the R12 models gradually approaches the asymptotic period spacing for long periods. On the other hand, the comparison between the periods of our models and the ones of the R12 models indicates differences from ∼20 s to ∼45 s for modes of equal radial order, calculated on models of WDs with equal mass, effective temperature, and H-layer thickness. The differences in the periods and period spacings are due to several improvements we have made in modeling the evolution of WD progenitors (i.e., the treatment

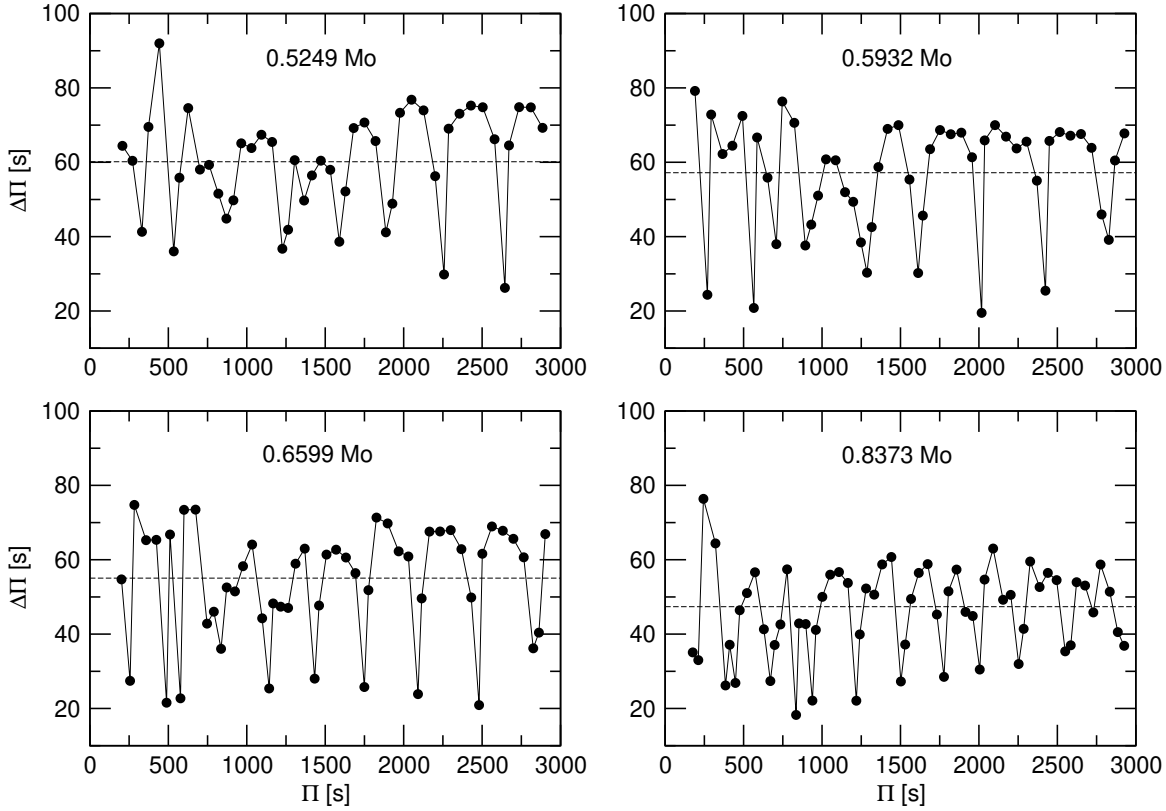

Fig. 14. Dipole ($\ell = 1$) forward period spacing versus periods for our template DA WD models with ultra-thin H envelopes ($\log(M_{\rm H}/M_\star) \sim -13.4$). The asymptotic period spacing for both sets of models is plotted with dashed lines.

of core He burning), as well as in the evolution during the WD stage, such as the Ne diffusion and the Coulomb sedimentation. These differences in the periods and period spacings likely have the important consequence that the parameters of ZZ Ceti stars derived through asteroseismological period-to-period fits up to date could substantially vary if our new set of models were used. Furthermore, our models include extremely thin H envelopes, $\log(M_{\rm H}/M_\odot) = -13.5$, ten thousand times thinner than the thinnest H envelopes considered in R12, $\log(M_{\rm H}/M_\odot) \sim -9.3$. This improvement paves the way for revisiting the asteroseismological determinations made so far considering the possibility that some ZZ Cetis can harbour ultra-thin H envelopes.

We close the paper by emphasizing that the new high-quality photometric observations provided by already completed space missions such as *Kepler*/K2 (Borucki et al. 2010; Howell et al. 2014), ongoing space programs such as TESS (Ricker et al. 2015) and Cheops (Moya et al. 2018), and future space telescopes such as Plato (Piotto 2018) pose a challenge to WD modeling teams, who must substantially improve stellar models so that they can be used in high-precision WD asteroseismology. The development of a new generation of detailed evolutionary models of DA WDs to interpret the new observations constitutes the first step in that direction – and this is the primary objective of this paper. Our future works will be focused on the calculation of a huge grid of stellar models and their adiabatic g-mode periods, and their application in asteroseismological analyses of the ZZ Cetis already known, as well as of the new ones that are to be discovered in the near future.

Acknowledgements. We acknowledge the suggestions and comments of an anonymous referee that improved the original version of this paper. Part of this work was supported by PICT-2017-0884 from ANPCyT, PIP 112-200801-00940 grant from CONICET, grant G149 from University of La Plata. This research has made use of NASA Astrophysics Data System.

References

Aerts, C. 2021, Rev. Mod. Phys., 93, 015001
Althaus, L. G., Serenelli, A. M., Córsico, A. H., & Montgomery, M. H. 2003, A&A, 404, 593
Althaus, L. G., Serenelli, A. M., Panei, J. A., et al. 2005, A&A, 435, 631
Althaus, L. G., Córsico, A. H., Bischoff-Kim, A., et al. 2010a, ApJ, 717, 897
Althaus, L. G., Córsico, A. H., Isern, J., & García-Berro, E. 2010b, A&ARv, 18, 471
Althaus, L. G., García-Berro, E., Renedo, I., et al. 2010c, ApJ, 719, 612
Althaus, L. G., Camisassa, M. E., Miller Bertolami, M. M., Córsico, A. H., & García-Berro, E. 2015, A&A, 576, A9
Althaus, L. G., Córsico, A. H., & De Gerónimo, F. 2020a, A&A, 644, A55
Althaus, L. G., Córsico, A. H., Uzundag, M., et al. 2020b, A&A, 633, A20
Beznogov, M. V., & Yakovlev, D. G. 2013, Phys. Rev. Lett., 111, 161101
Bischoff-Kim, A., Montgomery, M. H., & Winget, D. E. 2008, ApJ, 675, 1505
Bischoff-Kim, A., Østensen, R. H., Hermes, J. J., & Provencal, J. L. 2014, ApJ, 794, 39
Bischoff-Kim, A., Provencal, J. L., Bradley, P. A., et al. 2019, ApJ, 871, 13
Bognár, Z., Paparó, M., Molnár, L., et al. 2016, MNRAS, 461, 4059
Borucki, W. J., Koch, D., Basri, G., et al. 2010, Science, 327, 977
Bradley, P. A. 1998, ApJS, 116, 307
Bradley, P. A. 2001, ApJ, 552, 326
Brassard, P., Fontaine, G., Wesemael, F., & Tassoul, M. 1992, ApJS, 81, 747
Bravo, E., Isern, J., Canal, R., & Labay, J. 1992, A&A, 257, 534
Calcaferro, L. M., Córsico, A. H., & Althaus, L. G. 2017, A&A, 607, A33
Camisassa, M. E., Althaus, L. G., Córsico, A. H., et al. 2016, ApJ, 823, 158
Castanheira, B. G., & Kepler, S. O. 2009, MNRAS, 396, 1709
Catelan, M., & Smith, H. A. 2015, Pulsating Stars (Wiley-VCH)
Chang, P., Bildsten, L., & Arras, P. 2010, ApJ, 723, 719
Chen, J., Ferraro, F. R., Cadelano, M., et al. 2021, Nat. Astron., 5, 1170
Chidester, M. T., Timmes, F. X., Schwab, J., et al. 2021, ApJ, 910, 24
Christensen-Dalsgaard, J., Silva Aguirre, V., Cassisi, S., et al. 2020, A&A, 635, A165
Córsico, A. H. 2020, Front. Astron. Space Sci., 7, 47

Córsico, A. H. 2022, ArXiv e-prints [arXiv:2203.03769]
Córsico, A. H., & Althaus, L. G. 2005, A&A, 439, L31
Córsico, A. H., & Althaus, L. G. 2006, A&A, 454, 863
Córsico, A. H., Althaus, L. G., Kepler, S. O., Costa, J. E. S., & Miller Bertolami, M. M. 2008, A&A, 478, 869
Córsico, A. H., Althaus, L. G., Miller Bertolami, M. M., & Bischoff-Kim, A. 2012, A&A, 541, A42
Córsico, A. H., Althaus, L. G., Miller Bertolami, M. M., & Kepler, S. O. 2019, A&ARv, 27, 7
De Gerónimo, F. C., Althaus, L. G., Córsico, A. H., Romero, A. D., & Kepler, S. O. 2017, A&A, 599, A21
De Gerónimo, F. C., Althaus, L. G., Córsico, A. H., Romero, A. D., & Kepler, S. O. 2018, A&A, 613, A46
Deloye, C. J., & Bildsten, L. 2002, ApJ, 580, 1077
Fu, J.-N., Dolez, N., Vauclair, G., et al. 2013, MNRAS, 429, 1585
Gaia Collaboration (Prusti, T., et al.) 2016, A&A, 595, A1
García-Berro, E., Torres, S., Althaus, L. G., et al. 2010, Nature, 465, 194
Giammichele, N., Charpinet, S., Brassard, P., & Fontaine, G. 2017a, A&A, 598, A109
Giammichele, N., Charpinet, S., Fontaine, G., & Brassard, P. 2017b, ApJ, 834, 136
Giammichele, N., Charpinet, S., Fontaine, G., et al. 2021, MNRAS, submitted [arXiv:2106.15701]
Howell, S. B., Sobeck, C., Haas, M., et al. 2014, PASP, 126, 398
Kurtz, D. 2022, Annual Conf. and General Assembly of the African Astronomical Society, 60
Metcalfe, T. S., Salaris, M., & Winget, D. E. 2002, ApJ, 573, 803
Miller Bertolami, M. M. 2016, A&A, 588, A25
Moya, A., Barceló Forteza, S., Bonfanti, A., et al. 2018, A&A, 620, A203
Piotto, G. 2018, European Planetary Science Congress, EPSC2018-969
Renedo, I., Althaus, L. G., Miller Bertolami, M. M., et al. 2010, ApJ, 717, 183
Ricker, G. R., Winn, J. N., Vanderspek, R., et al. 2015, J. Astron. Telesc. Instrum. Syst., 1, 014003
Romero, A. D., Córsico, A. H., Althaus, L. G., et al. 2012, MNRAS, 420, 1462
Romero, A. D., Kepler, S. O., Córsico, A. H., Althaus, L. G., & Fraga, L. 2013, ApJ, 779, 58
Romero, A. D., Córsico, A. H., Castanheira, B. G., et al. 2017, ApJ, 851, 60
Romero, A. D., Kepler, S. O., Hermes, J. J., et al. 2022, MNRAS, 511, 1574
Salaris, M., Althaus, L. G., & García-Berro, E. 2013, A&A, 555, A96
Silva Aguirre, V., Christensen-Dalsgaard, J., Cassisi, S., et al. 2020, A&A, 635, A164
Tassoul, M., Fontaine, G., & Winget, D. E. 1990, ApJS, 72, 335
Unno, W., Osaki, Y., Ando, H., Saio, H., & Shibahashi, H. 1989, Nonradial Oscillations of Stars (Tokyo: University of Tokyo Press)
Werner, K., & Herwig, F. 2006, PASP, 118, 183
Winget, D. E., & Kepler, S. O. 2008, ARA&A, 46, 157